Research Square

Preprints are preliminary reports that have not undergone peer review.
They should not be considered conclusive, used to inform clinical practice,
or referenced by the media as validated information.

# Type I interferon signaling mediates silica-induced pulmonary B1 cell recruitment and autoimmunity

**Wilmot Juliet**

juliet.wilmot@uclouvain.be

UCLouvain

**Maxime-Loïc Mutshipay-Nkashama**

UCLouvain

**Colienne de Brouchoven de Bergeyck**

UCLouvain

**Saloua Ibouraadaten**

UCLouvain

**Francine Uwambayinema**

UCLouvain

**Yousof Yakoub**

UCLouvain

**Caroline Bouzin**

UCLouvain

**Davide Brusa**

UCLouvain

**Riccardo Leinardi**

UCLouvain

**François Huaux**

UCLouvain

**Research Article**

**Keywords:** Systemic Autoimmunity, Particulate Matter, Crystalline Silica, Type I Interferon (IFN-I), B1 Cells, CXCL13/CXCR5 Axis, Lung-to-Systemic Transition, Immune Dysregulation

**Posted Date:** November 13th, 2026

**DOI:** https://doi.org/10.21203/rs.3.rs-11403486/v1

**License:** This work is licensed under a Creative Commons Attribution 4.0 International License.
Read Full License

**Additional Declarations:** No competing interests reported.

# Type I interferon signaling mediates silica-induced pulmonary B1 cell recruitment and autoimmunity

*Wilmot Juliet[1], Mutshipay-Nkashama Maxime-Loïc[1], de Brouchoven de Bergeyck Colienne[1], Ibouraadaten Saloua[1], Uwambayinema Francine[1], Yakoub Yousof[1], Bouzin Caroline[2], Brusa Davide[3], Leinardi Riccardo[1], Huaux François[1].*

***Corresponding author**: Wilmot Juliet; juliet.wilmot@uclouvain.be*

[1]Louvain Centre for Toxicology and Applied Pharmacology (LTAP), Institute of Experimental and Clinical Research (IREC), Université Catholique de Louvain, Brussels, Belgium.

[2]2IP-IREC Imaging Platform, Institute of Experimental and Clinical Research, Université Catholique de Louvain, Brussels, Belgium.

[3]CytoFlux-Flow Cytometry Platform and Cell Sorting, Institute of Experimental and Clinical Research, Université catholique de Louvain, Bruxelles, Belgium.

## Abstract

**Background.** Environmental exposure to airborne particulate matter is a major contributor to pulmonary diseases, with growing epidemiological evidence linking inhalation of particles such as crystalline silica to systemic autoimmune diseases (AIDs). However, the molecular mechanisms responsible for the transition from silica-induced pulmonary inflammation to systemic loss of immune tolerance remain poorly understood. Given the established role of type I interferon (IFN-I) in systemic autoimmunity, we therefore investigated whether IFN-I signaling drives the development of silica-induced pulmonary inflammation to systemic autoimmune responses.

**Results.** Our study demonstrates that silica exposure induces a sustained IFN-I signature in wild-type (WT) mice, accompanied by increased pulmonary and circulating levels of anti-dsDNA, class-switched IgG autoantibodies, natural IgM and IgA. These humoral immune alterations are markedly attenuated in IFN-I receptor-deficient (*Ifnar1*$^{-/-}$) mice, demonstrating a critical role for IFN-I signaling in particle-induced autoimmunity. Silica exposure specifically triggered the recruitment of innate-like B1 cells to the injured lungs. In the absence of IFNAR, pulmonary B1-cell accumulation was markedly reduced, whereas B1 cells accumulated in the tracheobronchial lymph nodes and spleen, indicating that IFN-I signaling promotes their preferential recruitment to the lungs following silica injury. Mechanistically, silica exposure induced the CXCL13/CXCR5 chemotactic axis in WT mice, whereas this response was abolished in *Ifnar1*$^{-/-}$ mice, an effect associated with impaired pulmonary recruitment of CXCR5$^{+}$ B1 cells.

**Conclusions.** Our findings identify sustained IFN-I signaling as a key molecular link between silica-induced lung injury, inflammation and systemic humoral autoimmunity. By promoting CXCL13-dependent recruitment of innate-like B1 cells to the injured lungs, IFN-I established a pathway connecting environmental particle exposure to systemic autoimmune responses.



**Keywords.** Systemic Autoimmunity, Particulate Matter, Crystalline Silica, Type I Interferon (IFN-I), B1 Cells, CXCL13/CXCR5 Axis, Lung-to-Systemic Transition, Immune Dysregulation.

## 1. Background

Environmental exposure to airborne pollutants represents a significant global health burden, accounting for over four million premature deaths annually [1, 2]. This number is projected to rise due to climate change and accelerating industrialization, which drives the excessive discharge of hazardous materials and the emergence of unidentified compounds in the air. Inhalation of reactive particles is associated with severe pulmonary pathologies including chronic inflammation, fibrosis, and cancer [3]. Beyond direct pulmonary damage, epidemiological evidence increasingly links the inhalation of inorganic particles to the onset of systemic autoimmune disorders (AIDs) including systemic lupus erythematosus (SLE), rheumatoid arthritis (RA), and systemic sclerosis (SSc) [4-6]. Notably, respirable crystalline silica is a well-established environmental trigger of systemic loss of immune tolerance, supported by evidence from both large human cohorts and well-characterized *in vivo* murine models [6-9]. Given that AIDs affect up to 10% of the global population, with incidence rising by 19% annually and that genomic studies account for less than half of disease susceptibility, elucidating the molecular mechanisms by which environmental pollutants bridge local tissue injury to systemic immune dysregulation is of paramount importance [10-13].

The classical paradigm of biopersistent particle toxicity and pathogenicity is centered on the "cycle of injury" involving alveolar macrophages. Phagocytosis triggers lysosomal destabilization and NLRP3 inflammasome activation, leading to IL-1-mediated inflammation and immunogenic cell death (ICD) [14-16]. This process leads to the release of endogenous damage-associated molecular patterns (DAMPs), notably extracellular self-DNA, which has previously been identified as a key driver of autoantibody production by plasma cells [17]. While the cGAS/STING pathway has been shown to sense this self-DNA and trigger an acute type I Interferon (IFN-I) response [18], the transition from this initial inflammatory burst to a persistent, systemic autoimmune state remains poorly characterized, despite the well-established role of chronic IFN-I signaling in the pathogenesis of various AIDs [19-21].

In this study, we examined the contribution of IFN-I signaling to silica-induced pulmonary inflammation and systemic humoral autoimmunity, with particular emphasis on pulmonary B-cell responses. To address this question, we compared pulmonary and systemic immune responses to silica exposure in wild-type (WT) and IFNAR-deficient (*Ifnar1*$^{-/-}$) mice.

## 2. Results

### 2.1. Silica-induced sustained pulmonary IFN-I signaling

Given that IFN-I response is a hallmark of chronic autoimmune diseases [19], we investigated whether this signaling axis is sustained in long-term responses to silica. To address this question, WT and IFN-I receptor-deficient 129/Sv mice were subjected to repeated exposure of respirable crystalline silica (4 × 1 mg over 1 month) and evaluated 6 months after the initial exposure to assess inflammatory, fibrotic, and autoimmune responses. Transcriptional analysis of lung homogenates revealed a robust and sustained upregulation of IFN-I–associated pathways, including the interferon-stimulated genes (ISGs) *Irf7, Ifih1* and *Oasl2* (Fig. 1). The expression of *Irf7, Ifih1*, and *Oasl2* was significantly abrogated in treated mice deficient for the IFN-I receptor, confirming that the observed ISG signature is strictly dependent on canonical IFNAR signaling. These data demonstrate that silica exposure induces sustained activation of the IFN-I pathway, providing a mechanistic basis for investigating its contribution to subsequent immune dysregulation and pathological outcomes.

### 2.2. Pulmonary inflammation following silica exposure requires IFN-I

We first assessed the impact of IFN-I signaling on chronic pulmonary inflammation and fibrosis. Flow cytometric analysis of lung single-cell suspensions revealed a significant recruitment of macrophages ($F4/80^+CD11c^+$) and granulocytes ($Ly6C^+Ly6G^+$) in silica-exposed *WT* mice, reflecting elevated levels of the pro-inflammatory cytokines IL-1α, IL-1β, and the chemokines CCL2 and CXCL1/KC within the bronchoalveolar lavage fluid (BALF) (Fig. 2A-B). In contrast, silica-exposed *Ifnar1*$^{-/-}$ mice exhibited a marked reduction in these inflammatory parameters, indicating that the chronic pulmonary inflammation is largely dependent on the IFN-I axis. This requirement did not extend to the fibrotic response. Indeed, fibrotic biomarkers such as total lung hydroxyproline content and the release of the Timp1 remained elevated in both *WT* and *Ifnar1*$^{-/-}$ mice following silica exposure (Fig. 2C). Furthermore, the expression of *Foxp3*, a marker for regulatory T cells implicated in the modulation of the fibrotic process, was not significantly reduced in *Ifnar1*$^{-/-}$ lungs compared to *WT* counterparts (Fig. 2C). These data demonstrate that while the IFN-I axis is a primary driver of chronic particle-induced inflammation, it is not required for the development of pulmonary fibrosis.

### 2.3. IFN-I drives silica-induced humoral autoimmunity

Given the dependence of long-term inflammation on IFN-I signaling, we next investigated whether this axis contributes to the development of local and systemic humoral autoimmunity. Anti-double-stranded DNA (anti-dsDNA) autoantibodies and immunoglobulin levels were quantified in BALF and serum from *WT* and *Ifnar1*$^{-/-}$

mice after silica treatment. The data presented in Figure 3A revealed that silica-treated WT mice exhibited a robust accumulation of BALF anti-dsDNA autoantibodies. This local autoimmune response was strongly attenuated in *Ifnar1-/-* mice (Fig. 3A). Concurrently, total IgG, IgM, and IgA levels were markedly elevated in the BALF of silica-exposed WT mice, whereas this response was drastically diminished in their *Ifnar1-/-* counterparts (Fig. 3B-D). Parallel to our findings in the lungs, long-term responses to silica in *WT* mice were characterized by a significant elevation of circulating anti-dsDNA autoantibodies in the serum (Fig. 3E), a hallmark of self-tolerance breakdown. This systemic response was accompanied by a marked increase in total IgG, IgM and IgA in *WT* mice (Fig. 3F-H). The production of anti-dsDNA autoantibodies was completely abolished in *Ifnar1*$^{-/-}$ mice, demonstrating that systemic autoantibody generation in response to silica is strictly dependent on IFNAR signaling. While total IgG levels were already lower in untreated *Ifnar1*$^{-/-}$ mice compared to *WT* counterparts, their silica-induced elevation was further significantly abrogated in *Ifnar1*$^{-/-}$ mice, indicating that the IFN-I axis is necessary to both maintain basal immunoglobulin levels and fully amplify the class-switching differentiation program. Furthermore, total IgM levels were strongly reduced in the *Ifnar1*$^{-/-}$ silica-treated mice compared to *WT* counterparts, alongside a trend toward reduced IgA levels. Collectively, these findings indicate that IFN-I signaling plays a central role in shaping natural antibody and class-switched immunoglobulin responses at both local and systemic sites and promotes the autoimmune response following silica exposure.

### 2.4. Silica-induced IFN-I promotes pulmonary recruitment of innate-like B1 lymphocytes

To identify the cellular basis underlying the dysregulated humoral response to silica, we next characterized B-cell populations, including conventional B2, innate-like B1, and plasma cells by flow cytometry. Conventional B2 cells participate in adaptive humoral immunity and differentiate into antibody-secreting plasma cells (PCs), particularly following germinal center responses. In contrast, B1 cells are innate-like lymphocytes characterized by self-renewal and an antibody repertoire enriched in polyreactive and autoreactive specificities. Among the B-cell subsets analyzed, innate-like B1 cells were selectively recruited to the injured lungs following silica exposure. Indeed, WT mice displayed a marked accumulation of pulmonary B1 cells following silica instillation, whereas this response was completely abolished in *Ifnar1*$^{-/-}$ mice, demonstrating its dependence on IFN-I signaling (Fig. 4A). In contrast, B2 cells did not accumulate following silica exposure (Fig. 4B) although their numbers were consistently lower in *Ifnar1*$^{-/-}$ mice under both basal and silica-treated conditions, indicating a role for IFN-I signaling in maintaining the pulmonary B2-cell compartment. Plasma cell numbers were unaffected by either silica exposure or genotype (Fig. 4C). Overall, these findings reveal two distinct functions of IFN-I signaling within the

pulmonary B-cell compartment: selective recruitment of innate-like B1 cells following silica exposure and maintenance of basal pulmonary B-cell homeostasis.

### 2.5. IFN-I deficiency triggers B1-cell accumulation in peripheral lymphoid organs

The reduced abundance of pulmonary B1 cells in *Ifnar1*$^{-/-}$ mice raised the question of whether this phenotype resulted from impaired B-cell development within peripheral lymphoid organs, or defective recruitment to the site of silica-induced injury. We therefore characterized B-cell populations in the tracheobronchial lymph nodes (TLNs), which drain the lungs, and in the spleen, a major reservoir for both conventional and innate-like B cells. In WT mice, silica exposure increased B1-cell numbers in the TLNs (Fig. 4D-F). Surprisingly, silica-exposed *Ifnar1*$^{-/-}$ mice exhibited increased numbers of B1 cells in the TLNs compared with WT mice, contrasting with their reduced abundance in the lungs (Fig. 4A). A similar pattern was observed in the spleen, where silica-exposed *Ifnar1*$^{-/-}$ mice also displayed increased B1-cell numbers compared with WT mice (Fig. 4G). These findings demonstrated that B1 cells accumulate in draining lymphoid tissues after treatment but fail to efficiently reach the injured pulmonary compartment in the absence of IFN-I signaling. Silica exposure also increased B2-cell and PC counts in the TLNs of WT mice; however, these responses were not significantly altered by IFNAR deficiency (Fig. 4D–F). In contrast, silica exposure did not substantially affect splenic B2 and PC-cell populations in WT mice, although a slight increase in splenic B2 cells was detected in silica-treated Ifnar1$^{-/-}$ mice (Fig. 4G-I). Collectively, these findings indicate that IFN-I signaling shapes B-cell distribution following silica exposure, with a specific role in promoting the recruitment of innate-like B1 cells to the injured lung.

### 2.6. The CXCL13/CXCR5 axis mediates pulmonary recruitment of B1 cells.

To elucidate the molecular mechanisms underlying defective B1 cell recruitment to the lungs of silica-treated *Ifnar1*$^{-/-}$ mice, we examined the CXCL13/CXCR5 chemokine axis, a pivotal pathway involved in B1 cell chemoattraction [22] and autoimmunity [23]. Silica exposure in *WT* mice induced a robust upregulation of CXCL13 at both the transcriptional and protein levels in the lungs (Fig. 5A-B). Consistently, pulmonary expression of CXCR5, its cognate receptor, was also significantly upregulated after silica (Fig. 5C). These effects were abolished in *Ifnar1*$^{-/-}$ mice, indicating that IFN-I signaling is an upstream signal for CXCL13 and CXCR5 in pulmonary environment. We next investigated CXCR5 expression among B-cell subsets. In WT mice, silica treatment selectively increased the number of CXCR5$^{+}$ B1 cells in the lungs, whereas this pulmonary accumulation was abolished in *Ifnar1*$^{-/-}$ mice (Fig. 5D). Conversely, CXCR5$^{+}$ B1 cells were present in increased numbers in the TLNs and spleen of silica-treated *Ifnar1*$^{-/-}$ mice (Fig. 5F–H), suggesting their retention in peripheral lymphoid

tissues and impaired recruitment to the injured lung in the absence of IFN-I signaling. In contrast to B1 cells, CXCR5 expression in conventional B2 cell compartment remained low and was not induced by silica in the lungs (Fig. 5E). In peripheral lymphoid organs, the absence of IFNAR did not affect $CXCR5^+$ B2-cell numbers (Fig. 5I). Together, these findings identify an IFN-I/CXCL13/CXCR5 axis that promotes the selective recruitment of innate-like B1 cells to the injured lung, thereby sustaining the systemic autoimmune response to chronic silica exposure.

## 3. Discussion

The association between silica exposure and systemic autoimmune diseases (AIDs) was first documented in 1914, with the observation of a high prevalence of scleroderma among stone masons [24]. Over the past century, respirable crystalline silica has become a well-established experimental model for investigating how inorganic particle exposure contributes to the development of AIDs, including systemic lupus erythematosus (SLE), rheumatoid arthritis (RA), and systemic sclerosis (SSc) [4, 5, 9]. Its capacity to induce a systemic loss of self-tolerance is now firmly established across both epidemiological cohorts and experimental murine models [6-8]. Recent work using the Collaborative Cross (CC) or diversity outbred (DO) mouse models, which mirror human genetic diversity, revealed that silica exposure can trigger *de novo* systemic autoimmunity [25, 26]. Concurrently, the severity of autoimmune outcomes, including systemic autoantibody production, local and systemic immune activation, inflammatory arthritis, and glomerular lesions, is significantly exacerbated upon silica exposure in pre-existing subclinical autoimmunity [25, 27-30]. These studies indicate that genetic background strongly influences the magnitude and spectrum of silica-induced autoimmune responses. However, despite over a hundred years of clinical observation, the cellular and molecular bridges connecting pulmonary particle deposition to systemic humoral breakdown have remained elusive.

In this context, our findings provide a novel mechanism linking inorganic particle-induced pulmonary inflammation to systemic loss of tolerance. We identify IFN-I signaling as a key determinant of pulmonary B1-cell accumulation and systemic autoantibody responses following silica exposure. Unlike conventional B2 cells, B1 cells are innate-like lymphocytes characterized by self-renewal and a repertoire enriched in polyreactive and autoreactive specificities, positioning them at the interface between innate and adaptive humoral immunity [22, 31]. Several studies have implicated B1 cells in systemic autoimmunity, including SLE, through antibody and cytokine production, interactions with T cells, and their capacity to migrate to inflamed tissues [32-34]. In silica-exposed *Ifnar1*$^{-/-}$ mice, pulmonary B1 cell recruitment is impaired. This local deficit is mirrored by a significant accumulation in the TLNs and the spleen. This suggests that IFN-I signaling is required to mobilize these rapid

responders toward the site of injury. The selective recruitment of B1 cells may contribute to the generation of naturally derived autoantibodies, including anti-dsDNA, which characterize the systemic loss of immune tolerance.

The reduced number of B2 cells in untreated *Ifnar1*$^{-/-}$ lungs further suggests that IFN-I signaling contributes to the homeostatic maintenance or localization of B cells within the pulmonary compartment. However, unlike B1 cells, pulmonary B2 cells did not increase following silica exposure, suggesting that their recruitment to the injured lungs is not a prominent feature of the response to silica. Importantly, silica exposure increased both B2-cell and PC populations in the lung-draining TLNs, and these responses were preserved in *Ifnar1*$^{-/-}$ mice. Thus, silica-induced B-cell responses are not restricted to IFN-I-dependent pulmonary accumulation of B1 cells. Rather, these findings indicate that silica also elicits B-cell responses within draining lymphoid tissues that may contribute to broader systemic humoral responses and potentially to extrapulmonary manifestations, including the renal involvement reported following silica exposure [7].

The recruitment of B cells to inflamed tissues is a highly coordinated process integrating multiple chemokine pathways, including CXCL12/CXCR4, CCL19-CCL21/CCR7, CXCL13/CXCR5, and CXCL9-11/CXCR3 axis [35, 36]. In this study, we specifically focused our investigation on the CXCL13/CXCR5 pathway because our data identified the B1 compartment as the primary target of IFN-I-dependent dysregulation. This focus is strongly supported by the unique chemotactic hierarchy of B1 cells which exhibit high CXCR5 expression and an absolute reliance on CXCL13, while showing little to no responsiveness to CCL19, CCL21, and CXCL12 [22]. Our findings therefore support a model in which silica-induced IFN-I signaling establishes a pulmonary CXCL13/CXCR5 chemotactic axis favoring the recruitment of CXCR5$^{+}$ B1 cells to the injured lung. Activation of CXCL13/CXCR5 axis has also been recently associated with the pathogenesis of several autoimmune diseases, such RA, SLE, SSc, and primary Sjögren's syndrome (pSS), diseases for which epidemiological evidence has increasingly linked inorganic particle inhalation as a risk factor [5, 6]. Beyond recruitment, CXCL13 is a key orchestrator of ectopic lymphoid-like structures (ELSs). These tertiary lymphoid organs can function as local germinal centers, promoting the maturation of autoreactive B cells and the production of autoantibodies [23]. The formation of such structures has been consistently documented in animal models of inorganic particle exposure [37-40] and we previously demonstrated that mouse innate-like B1 cells are essential promoters of inhaled particle-induced granuloma formation [40]. The pivotal role of IFN-I in pulmonary CXCL13 expression is further supported by findings in other inflammatory contexts. Denton et al. demonstrated that during Influenza A virus (IAV) infection, type I IFNs induce pulmonary CXCL13 expression, and that *Ifnar1*$^{-/-}$ mice exhibit a significant reduction in this chemokine

[41]. Our study extends this paradigm to particle-induced sterile inflammation and suggests that IFN-I-dependent induction of pulmonary CXCL13 may represent a shared mechanism across infectious and sterile inflammatory settings.

We also addressed the potential impact of host-intrinsic factors, such as sex and genetic background during silica-induced autoimmune responses. In human systemic AIDs, a strong female predominance is typically observed, often attributed to the ability of estrogens to prime the B cell compartment and enhance cytokine production [42]. Interestingly, in our model, both male and female mice exhibited comparable patterns of systemic immune activation following silica exposure (Supp. Fig.1), with no major sex-based difference in autoantibody levels as previously observed in other models [25]. Genetic deletion of IFNAR in female mice resulted in a marked loss of anti-dsDNA, IgG, and IgM responses (Supp. Fig.1), comparable to that observed in males. Furthermore, we evaluated this response across two genetically distinct landscapes: the 129sv strain, highly susceptible to interferon-driven pathology, and the C57BL/6 strain, more resistant. While the attenuation of autoantibody production was more pronounced in *Ifnar1*$^{-/-}$ mutants on the 129sv background than C57BL/6 (Supp. Fig. 2F), the fundamental requirement for IFN-I signaling remained consistent across both strains (Supp. Fig. 2). These findings underscore a critical paradigm in the study of the exposome: while genetic susceptibility and hormonal priming are traditional modifiers of disease severity, environmental insult, crystalline silica here, acts as a primary, dominant driver of pathogenesis. By triggering a conserved IFN-I-dependent pathway, silica exposure effectively overrides individual biological variability to initiate the systemic breakdown of self-tolerance.

Finally, our results allow for a clear decoupling of the different outcomes of silica exposure and further distinguish the pathways underlying the autoimmune and fibrotic consequences of silica exposure. Consistent with our previous work [43], we show that while the IFN-I axis dictates the chronic inflammatory and autoimmune response, it is not required for the development of pulmonary fibrosis. Our findings suggest that targeting IFN-I signaling, and potentially the CXCL13/CXCR5 axis, preferentially modulates the inflammatory and autoimmune consequences of silica exposure without necessarily altering the underlying fibrotic response. Accordingly, patients affected by autoimmune conditions secondary to silica exposure represent a promising cohort for targeted anti-IFN-I therapies. This distinction is crucial for the development of precision medicine approaches for individuals exposed to respirable crystalline silica.

## 4. Conclusions

In summary, our work establishes IFN-I signaling as a key molecular link between particle-induced pulmonary inflammation to systemic autoimmunity. We demonstrate that IFN-I promotes the pulmonary recruitment of $CXCR5^+$ B1 cells following silica exposure, in association with activation of the CXCL13/CXCR5 chemotactic axis and the development of systemic humoral autoimmune responses. By identifying IFN-I-dependent pulmonary B1-cell recruitment as a key component of this response, our findings provide new mechanistic insight into how chronic environmental particle exposure can promote systemic autoimmune disease.

## 5. Material & Methods

### 5.1. Mice and environmental conditions

Wild-type (*WT*) and *Ifnar1*$^{-/-}$ 129/Sv mice were obtained from the *Transgenose Institute* (CNRS, Orléans, France) [44]. C57BL/6 mice were purchased from Janvier SAS (St Berthevin, France). All mice were maintained in a Specific Pathogen-Free (SPF) facility. The mice were housed in polycarbonate cages with conventional sawdust (Carfil, Oud-Turnhout, Belgium) in a controlled environment (25 °C, 50 % relative humidity) with acidified water and food *ad libitum*. To limit silicon (Si) background in the tissues, a standard rodent diet low in Si was selected. All experimental processes were in accordance with the NIH Guide for the Care and Use of Laboratory animals, and Belgian and European regulations (EEC n ° 86/609, LA1230312 and 2022/UCL/MD/019). Animals were sacrificed via an intraperitoneal injection of 60 mg/ml (200 µl, intraperitoneal) sodium pentobarbital (Certa, Braine-l'Alleud, Belgium).

### 5.2. Experimental cohorts

For systemic inflammatory and molecular profiling (RT-qPCR, ELISA, and autoantibody detection), a mixed-sex cohort was used, comprising 30 *WT* (15 males, 15 females) and 40 *Ifnar1*$^{-/-}$ mice (20 males, 20 females) distributed as indicated in *table 1*. Data for male mice are presented in the main figures (Figs. 1–3), while corresponding data for female mice are provided in the Supplementary Information (Supp. Fig.1). For flow cytometry experiments (Figs 4-5), a dedicated cohort of 25 male mice (approx. 8 months old) was used, and distribution is described in *table 2*. Consequently, cross-platform comparisons were interpreted as complementary trends rather than direct individual-level correlations.

*Table 1.*

| | | | |
|---|---|---|---|
| 129SV WT | Males | NaCl | N = 6 |
| | | MinUSil | N = 9 |
| | Females | NaCl | N = 6 |
| | | MinUSil | N = 9 |
| 129SV *Ifnar1*$^{-/-}$ | Males | NaCl | N = 8 |
| | | MinUSil | N = 12 |
| | Females | NaCl | N = 8 |
| | | MinUSil | N = 12 |

*Table 2.*

| | | |
|---|---|---|
| 129SV WT | NaCl | N = 4 |
| | MinUSil | N = 5 |
| 129SV *Ifnar1*$^{-/-}$ | NaCl | N = 6 |
| | MinUSil | N = 10 |

### 5.3. Respirable Crystalline Silica (RCS) particles

Min-U-Sil-5 particles (U.S. Silica Co., Berkeley Springs, WV, USA; lot number 15062696) were supplied by the University of Turin. It is a commercial fractured microcrystalline α-quartz largely used in studies of experimental silicosis and/or lung cancer (IARC, 1996). Physico-chemical properties were deeply characterized in previous studies and are summarized in *table 3*.

*Table 3.*

| ***Origin (Type)*** | ***Surface State*** | ***Particle size (µm ± SD)*** | ***SSA ($m^2/g$)*** | ***NFS content*** | ***Ref*** |
|---|---|---|---|---|---|
| Commercial (α-quartz) | Fractured | 1.3 ± 0.6 | 4.3 | High | [14, 16] |

### 5.4. Particle dispersion for animal studies

The particles were heated at 200 °C for 2h just prior to suspension to inactivate any trace endotoxin. Stock suspensions prepared in 0.9 % NaCl were ultrasonicated on ice (3 min, 100 W, probe diameter 3 mm) using a VCX 750 ultrasonic processor (Sonics, Newtown, CT, USA) and then sonicated in a bath for 2 min to ensure dissociation of particle agglomerates (total delivered energy 27 kJ).

### 5.5. Silica treatment

Mice were exposed to crystalline silica via four weekly oropharyngeal instillations of 1 mg (50 µL per instillation in 0.9% NaCl, total dose of 4 mg). Control groups received an equal volume of sterile saline. Oropharyngeal aspiration (o.p.a.) was used as a non-surgical alternative to intratracheal instillation and offers improved reproducibility of pulmonary outcomes. To maximize pulmonary delivery and minimize accidental gastrointestinal exposure, the mice's tongues were gently extended with forceps to expose the oropharynx and obstruct the epiglottis. Their nostrils were occluded using forceps to promote oral inhalation and ensure direct fiber suspension aspiration into the lungs. Mice were continuously monitored during anesthesia and throughout recovery. Mice were euthanized six months after the initial exposure.

### 5.6. Blood, BAL, and organs collection for systemic inflammatory and molecular profiling

Mice blood was collected by cardiac puncture using non-heparinized sterile syringes and has been centrifugated at 2500 rpm at 20°C for 10 min. The resulting serum was carefully extracted and transferred into 1,5 mL tubes, which were subsequently stored at -80°C until analysis. Bronchoalveolar lavage (BAL) was performed post-euthanasia, the lungs were perfused with 0.9 % NaCl, and the trachea was cannulated. The recovered bronchoalveolar lavage fluid (BALF) was then centrifuged (280 x g, 10 min, 4 °C; Centrifuge 5804 R, Eppendorf, Hamburg, Germany). The cell-free supernatant was collected and stored at −80 °C for subsequent biochemical measurements. After BAL collection, whole lungs were surgically excised via a midline sternotomy. Spleen and tracheobronchial lymph nodes (TLNs) were then dissected under sterile conditions. Lungs, spleen, and TLNs were promptly homogenized in 2 ml ice-cold PBS using an Ultra-Turrax T25 homogenizer (Janke and Kunkel, Brussels, Belgium) and stored at −80 °C for further analysis.

### 5.7. Organs collection for flow cytometry

Single-cell suspensions were prepared from the lungs, spleens, and TLNs of the dedicate male flow cytometry cohort (n=25). All procedures were performed under sterile conditions, and samples were strictly maintained on ice or at 4°C unless otherwise stated to ensure maximal cell viability.

*Spleen and TLNs.*

Following dissection, spleens and TLNs were immediately immersed in ice-cold Hanks Balanced Salt Solution (HBSS 1x, Gibco, 24020117) supplemented with 2% fetal bovine serum (FBS, Gibco, A5256701) and 1% antibiotics-antimycotics (Gibco, 15240062). Tissues were mechanically dissociated by mashing through a 70 µm cell strainer (Falcon) using a 10 mL syringe plunger. The resulting cell suspensions were adjusted with HBSS +

2% FBS and centrifuged (350–400 x g, 5 min, 4°C). To remove red blood cells, cell pellets were resuspended in 1 mL of ACK lysing buffer (Gibco, A1049201), or adjusted volume for TLNs and incubated for 3 min at room temperature. The reaction was quenched by adding 9 mL of ice-cold HBSS, followed by centrifugation (350–400 x g, 5–7 min, 4°C). Final cell pellets were resuspended in FACS buffer (PBS 1x, 2% FBS, 2 mM EDTA).

*Lung tissue.*

Lung single-cell dissociation required an initial enzymatic digestion step. Immediately after euthanasia, the trachea was cannulated, and 1 mL of an enzymatic cocktail (20 mg/mL Pronase and 1 mg/mL DNase I in HBSS, pre-incubated for 20 min at 37°C) was intratracheally injected. Lungs were then excised and placed in 3 mL of FBS at room temperature to maintain enzymatic activity. Tissues were mechanically homogenized using repeated passes through a 20 mL syringe and subsequently incubated at 37°C to complete the digestion. Following incubation, the suspension volume was adjusted to 10 mL with HBSS and filtered through a 70 µm cell strainer. Residual tissue fragments were mashed on the filter and rinsed with HBSS to maximize cell recovery. The filtrate was centrifuged (350–400 x g, 7 min, 4°C), washed, and the final cell pellet was resuspended in FACS buffer.

For all organs, cell suspensions were visually inspected for aggregates, and cell concentrations were determined by trypan blue exclusion using a Neubauer hemocytometer prior to flow cytometry staining.

### 5.8. Evaluation of long-term responses in the BALF of mice.

Pro-inflammatory cytokines were quantified in BALF samples at 6 months endpoint using DuoSet ELISA kits (R&D Systems, Minneapolis, USA): IL-1α (Cat. # DY400), IL-1β (Cat. # DY401), IL-6 (Cat. # DY406), TNF-α (Cat. # DY410), CXCL1 (Cat. # DY453), CCL2 (Cat. # DY479), TIMP1 (Cat. # DY980). All measurements were performed in strict accordance with the providers' guidelines.

### 5.9. Hydroxyproline measurements.

Hydroxyproline lung content was measured by high performance liquid chromatography after hydrolysis of the lung tissue in 6 N HCl as reported previously [45, 46].

### 5.10. Humoral markers measure in serum and BALF.

BALF and serum levels of anti-dsDNA IgG were quantified using the LBIS Mouse anti-dsDNA ELISA kit (Cat #637-02691) according to the manufacturer’s instructions. Total IgM, IgA, and IgG concentrations were measured in BALF and in serum using specific mouse uncoated ELISA kits from Invitrogen (Cat #88-50470, #88-50450, and #88-50400, respectively). All absorbance measurements and protocols were performed in strict accordance with the providers' guidelines.

### 5.11. Flow Cytometry

*Cell Surface Staining.*

Single-cell suspensions were adjusted to $10^6$ cells per tube in FACS buffer (calcium/magnesium-free PBS, 2% FBS, 2 mM EDTA). To prevent non-specific binding, Fc receptors were blocked using anti-CD16/32 (Fc Block, BD Biosciences) for 20 min at 4°C in the dark. Cells were then incubated for 20 min at 4°C with a 12-color fluorochrome-conjugated antibody cocktail (*Table 4*). All antibodies were used at a 1:200 dilution unless otherwise specified. Following incubation, cells were washed, centrifuged (400 x g, 5 min, 4°C), and resuspended in 300 µL of FACS buffer. DAPI (dil 1:150) was added immediately before acquisition to exclude dead cells.

*Table 4.*

| Markers | Fluorochrome | Clone | Company | Catalog Ref |
|---|---|---|---|---|
| **CD45** | FITC | S18009F | BioLegend | 157214 |
| **CD45R/B220** | BV785 | RA3-6B2 | BioLegend | 103245 |
| **CD19** | RY586 | 1D3 | BD Biosciences | 753680 |
| **CD11c** | RB613 | N418 | BD Biosciences | 758187 |
| **Ly6G** | BV510 | 1A8 | BioLegend | 127633 |
| **Ly6C** | Spark Blue 574 | HK1.4 | BioLegend | 285177 |
| **F4/80** | BV605 | BM8 | BioLegend | 123133 |
| **CD3** | BV650 | 17A2 | BioLegend | 100229 |
| **CD4** | BV711 | GK1.5 | BioLegend | 100447 |
| **CD8a** | RY610 | 53-6.7 | BD Biosciences | 571144 |
| **CD43** | APC | S11 | BioLegend | 143208 |
| **CD138** | Spark Red 718 | 281-2 | BioLegend | 285205 |
| **CXCR5 (CD185)** | APC-Cy7 | L138D7 | BioLegend | 145526 |
| **Fc block (anti-CD16/32)** | - | 2.4G2 | BD Biosciences | 553142 |
| **DAPI** | - | - | Invitrogen | 0000216561 |

*Data Acquisition and Analysis.*

Data were acquired on a NovoCyte flow cytometer (Agilent) and analyzed using NovoExpress software. Spectral overlap was corrected using single-stain compensation beads, and Fluorescence Minus One (FMO) were employed to define gating boundaries for markers with low or heterogenous expression, including CD138, and CXCR5.

*Gating Strategy.*

A systematic gating hierarchy was applied across all organs (Supplementary Fig. 3). Briefly, total leukocytes were identified by FSC-A/SSC-A, followed by doublet exclusion (FSC-H vs. FSC-A) and dead cell exclusion ($DAPI^-$). Live total leukocytes were identified as $CD45^+$. Within $CD45^+$ population, Granulocytes and Monocytes were discriminated using Ly6G and Ly6C. Inside granulocytes gate, macrophages and neutrophiles were defined by F4/80, CD64 and CD11c. From double negative L6G/Ly6C population, T cells were identified as $CD4^+/CD8^+$, while Dendritic cells were gated as $CD11c^+$. Following these exclusions, B lymphocytes were identified as $CD19^+$, and remaining plasma cells (PC) were excluded with CD138 due to their dim expression in CD19 ($CD19^{low/-}$ $CD4^-$ $CD8^-$ $CD138^+$). B cell compartments were discriminated based on CD43 expression, B-1 cells ($CD43^+$), and B-2 cells ($CD43^-$). The frequency of CXCR5 was quantified within each specific B cell subset (Supplementary Fig 3).

### 5.12. Statistical analysis

The sample size (n) of each experimental group is described in *table 1* and *table 2*. Results from each group were averaged and expressed as means + standard error of the mean (s.e.m., represented as error bars). T-test was used for comparison between 2 groups and one-way ANOVA analysis was used for comparisons among 3 or more groups. Two-way ANOVA analysis was used to examine the influence of two different independent variables. The Statistics program Prism (GraphPad Prism 9) was used for analysis. Statistical significance was set at a P–value < 0.05.

## 6. Declarations

### 6.1. Funding Declaration

This study was supported by a FRIA/FNRS grant (Grant ID: 40038001), by *Fonds de la Recherche Scientifique* (FNRS) and by *Actions de Recherche Concertées* (FWB, Grant ID: ARC 19/24-098, CYTAID).

### 6.2. Data Availability

Not applicable.

### 6.3. Consent for publication

Not applicable.

### 6.4. Competing Interest

The authors declare no competing interests.

### 6.5. Animal Ethics declaration

All experimental processes were in accordance with the NIH Guide for the Care and Use of Laboratory animals, and Belgian and European regulations (EEC n ° 86/609, LA1230312 and 2022/UCL/MD/019).

### 6.6. Author Contributions Statement

J.W. and F.H. wrote the main manuscript text. J.W., M.M., C.B., S.I., F.U. and Y.Y. contributed to the production of the experimental data. D.B., C.B. and R.L. provided technical and theoretical expertise. All authors reviewed the manuscript.

## 7. References


1. Cohen, A.J., et al., *Estimates and 25-year trends of the global burden of disease attributable to ambient air pollution: an analysis of data from the Global Burden of Diseases Study 2015.* Lancet, 2017. **389**(10082): p. 1907–1918.
2. (WHO), W.H.O. *Ambient (outdoor) air pollution*. 2024 [cited 2026 22.05]; Available from: https://www.who.int/news-room/fact-sheets/detail/ambient-(outdoor)-air-quality-and-health.
3. IARC, *Arsenic, metals, fibres, and dusts.* IARC Monogr Eval Carcinog Risks Hum 2012, 2012: p. 100(Pt C):11–465.
4. Miller, F.W., et al., *Epidemiology of environmental exposures and human autoimmune diseases: findings from a National Institute of Environmental Health Sciences Expert Panel Workshop.* J Autoimmun, 2012. **39**(4): p. 259–71.
5. Zhao, C.N., et al., *Emerging role of air pollution in autoimmune diseases.* Autoimmun Rev, 2019. **18**(6): p. 607–614.
6. Boudigaard, S.H., et al., *Occupational exposure to respirable crystalline silica and risk of autoimmune rheumatic diseases: a nationwide cohort study.* Int J Epidemiol, 2021. **50**(4): p. 1213–1226.
7. Janssen, L.M.F., et al., *Exposure to silicates and systemic autoimmune-related outcomes in rodents: a systematic review.* Part Fibre Toxicol, 2022. **19**(1): p. 4.
8. Morin, L., V. Lecureur, and A. Lescoat, *Results from omic approaches in rat or mouse models exposed to inhaled crystalline silica: a systematic review.* Part Fibre Toxicol, 2024. **21**(1): p. 10.
9. Pollard, K.M., *Silica, Silicosis, and Autoimmunity.* Front Immunol, 2016. **7**: p. 97.
10. Kumar, M., et al., *Autoimmune disease: genetic susceptibility, environmental triggers, and immune dysregulation. Where can we develop therapies?* Front Immunol, 2025. **16**: p. 1626082.
11. Lerner, A., P. Jeremias, and T. Matthias, *The World Incidence and Prevalence of Autoimmune Diseases is Increasing.* International Journal of Celiac Disease, 2016. **3**(4): p. 151–155.
12. Miller, F.W., *The increasing prevalence of autoimmunity and autoimmune diseases: an urgent call to action for improved understanding, diagnosis, treatment, and prevention.* Curr Opin Immunol, 2023. **80**: p. 102266.
13. Manolio, T.A., et al., *Finding the missing heritability of complex diseases.* Nature, 2009. **461**(7265): p. 747–53.
14. Leinardi, R., et al., *Gasdermin D membrane pores orchestrate IL-1alpha secretion from necrotic macrophages after NFS-rich silica exposure.* Arch Toxicol, 2023. **97**(4): p. 1001–1015.
15. Liu, Q., et al., *Alveolar macrophages initiate the spatially targeted recruitment of neutrophils after nanoparticle inhalation.* Sci Adv, 2025. **11**(45): p. eadx8586.

16. Pavan, C., et al., *Nearly free surface silanols are the critical molecular moieties that initiate the toxicity of silica particles*. Proc Natl Acad Sci U S A, 2020. **117**(45): p. 27836–27846.
17. Leinardi, R., C. Longo Sanchez-Calero, and F. Huaux, *Think Beyond Particle Cytotoxicity: When Self-Cellular Components Released After Immunogenic Cell Death Explain Chronic Disease Development*. Front Toxicol, 2022. **4**: p. 887228.
18. Benmerzoug, S., et al., *STING-dependent sensing of self-DNA drives silica-induced lung inflammation*. Nat Commun, 2018. **9**(1): p. 5226.
19. Choubey, D. and K.D. Moudgil, *Interferons in autoimmune and inflammatory diseases: regulation and roles*. J Interferon Cytokine Res, 2011. **31**(12): p. 857–65.
20. Banchereau, J. and V. Pascual, *Type I interferon in systemic lupus erythematosus and other autoimmune diseases*. Immunity, 2006. **25**(3): p. 383–92.
21. Hall, J.C. and A. Rosen, *Type I interferons: crucial participants in disease amplification in autoimmunity*. Nat Rev Rheumatol, 2010. **6**(1): p. 40–9.
22. Ansel, K.M., R.B. Harris, and J.G. Cyster, *CXCL13 is required for B1 cell homing, natural antibody production, and body cavity immunity*. Immunity, 2002. **16**(1): p. 67–76.
23. Pan, Z., et al., *Role of the CXCL13/CXCR5 Axis in Autoimmune Diseases*. Front Immunol, 2022. **13**: p. 850998.
24. Bramwell, B., *Diffuse scleroderma: its frequency; its occurrence in stone masons; its treatment by fibrolysis in elevations of temperature due to fibrolysis injections*. Edinb Med J Edinb Med J 1914.
25. Janssen, L.M.F., et al., *Crystalline silica exposure induces multiple systemic autoimmune phenotypes including inflammatory arthritis and nephritis in Collaborative Cross mice with differing sub-clinical autoimmune profiles*. bioRxiv, 2025.
26. Mayeux, J.M., et al., *Silicosis and Silica-Induced Autoimmunity in the Diversity Outbred Mouse*. Front Immunol, 2018. **9**: p. 874.
27. Janssen, L.M.F., et al., *Silica-mediated exacerbation of inflammatory arthritis: A novel murine model*. bioRxiv, 2025.
28. Janssen, L.M., et al., *Differential pulmonary toxicity and autoantibody formation in genetically distinct mouse strains following combined exposure to silica and diesel exhaust particles*. Part Fibre Toxicol, 2024. **21**(1): p. 8.
29. Brown, J.M., J.C. Pfau, and A. Holian, *Immunoglobulin and lymphocyte responses following silica exposure in New Zealand mixed mice*. Inhal Toxicol, 2004. **16**(3): p. 133–9.
30. Zhang, P., et al., *Dioscin ameliorates silica-aggravated systemic lupus erythematosus via suppressing apoptosis and improving LC3-associated phagocytosis in MRL/lpr mice*. Int Immunopharmacol, 2023. **116**: p. 109814.
31. Hieronimus, L. and F. Huaux, *B-1 cells in immunotoxicology: Mechanisms underlying their response to chemicals and particles*. Front Toxicol, 2023. **5**: p. 960861.
32. Morris, G., et al., *Emerging role of innate B1 cells in the pathophysiology of autoimmune and neuroimmune diseases: Association with inflammation, oxidative and nitrosative stress and autoimmune responses*. Pharmacol Res, 2019. **148**: p. 104408.
33. Xu, Z. and L. Morel, *Contribution of B-1a cells to systemic lupus erythematosus in the NZM2410 mouse model*. Ann N Y Acad Sci, 2015. **1362**(1): p. 215–23.
34. She, Z., et al., *The Role of B1 Cells in Systemic Lupus Erythematosus*. Front Immunol, 2022. **13**: p. 814857.
35. Chen, K., et al., *Chemokines in homeostasis and diseases*. Cell Mol Immunol, 2018. **15**(4): p. 324–334.
36. Cyster, J.G. and C.D.C. Allen, *B Cell Responses: Cell Interaction Dynamics and Decisions*. Cell, 2019. **177**(3): p. 524–540.

37. Janssen, L.M.F., et al., *Susceptibility to systemic autoimmunity rather than the presence of the HLA-DR4 peptide binding domain alone leads to severe inflammatory arthritis following inhalation of crystalline silica.* Part Fibre Toxicol, 2026. **23**(1).
38. Bates, M.A., et al., *Silica Triggers Inflammation and Ectopic Lymphoid Neogenesis in the Lungs in Parallel with Accelerated Onset of Systemic Autoimmunity and Glomerulonephritis in the Lupus-Prone NZBWF1 Mouse.* PLoS One, 2015. **10**(5): p. e0125481.
39. Foster, M.H., et al., *Silica Exposure Differentially Modulates Autoimmunity in Lupus Strains and Autoantibody Transgenic Mice.* Front Immunol, 2019. **10**: p. 2336.
40. Hieronimus, L., et al., *Mouse innate-like B-1 lymphocytes promote inhaled particle-induced in vitro granuloma formation and inflammation in conjunction with macrophages.* Arch Toxicol, 2022. **96**(2): p. 585–599.
41. Denton, A.E., et al., *Type I interferon induces CXCL13 to support ectopic germinal center formation.* J Exp Med, 2019. **216**(3): p. 621–637.
42. Whitacre, C.C., *Sex differences in autoimmune disease.* Nat Immunol, 2001. **2**(9): p. 777–80.
43. Giordano, G., et al., *Type I interferon signaling contributes to chronic inflammation in a murine model of silicosis.* Toxicol Sci, 2010. **116**(2): p. 682–92.
44. Muller, U., et al., *Functional role of type I and type II interferons in antiviral defense.* Science, 1994. **264**(5167): p. 1918–21.
45. Driscoll, K.E., et al., *Stimulation of rat alveolar macrophage fibronectin release in a cadmium chloride model of lung injury and fibrosis.* Toxicol Appl Pharmacol, 1992. **116**(1): p. 30–7.
46. Huaux, F., et al., *A profibrotic function of IL-12p40 in experimental pulmonary fibrosis.* J Immunol, 2002. **169**(5): p. 2653–61.

## Figures

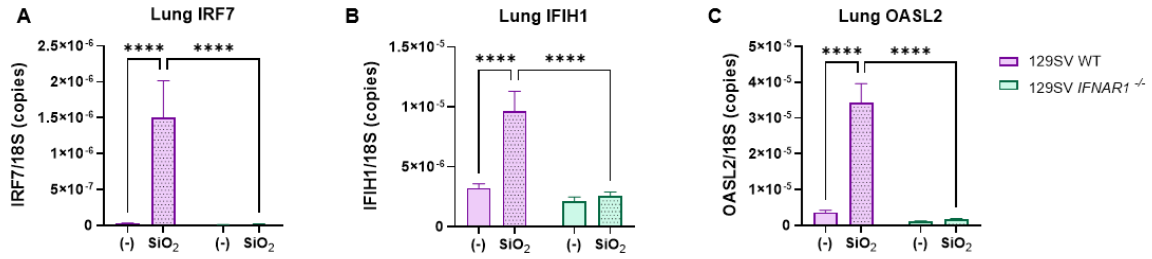
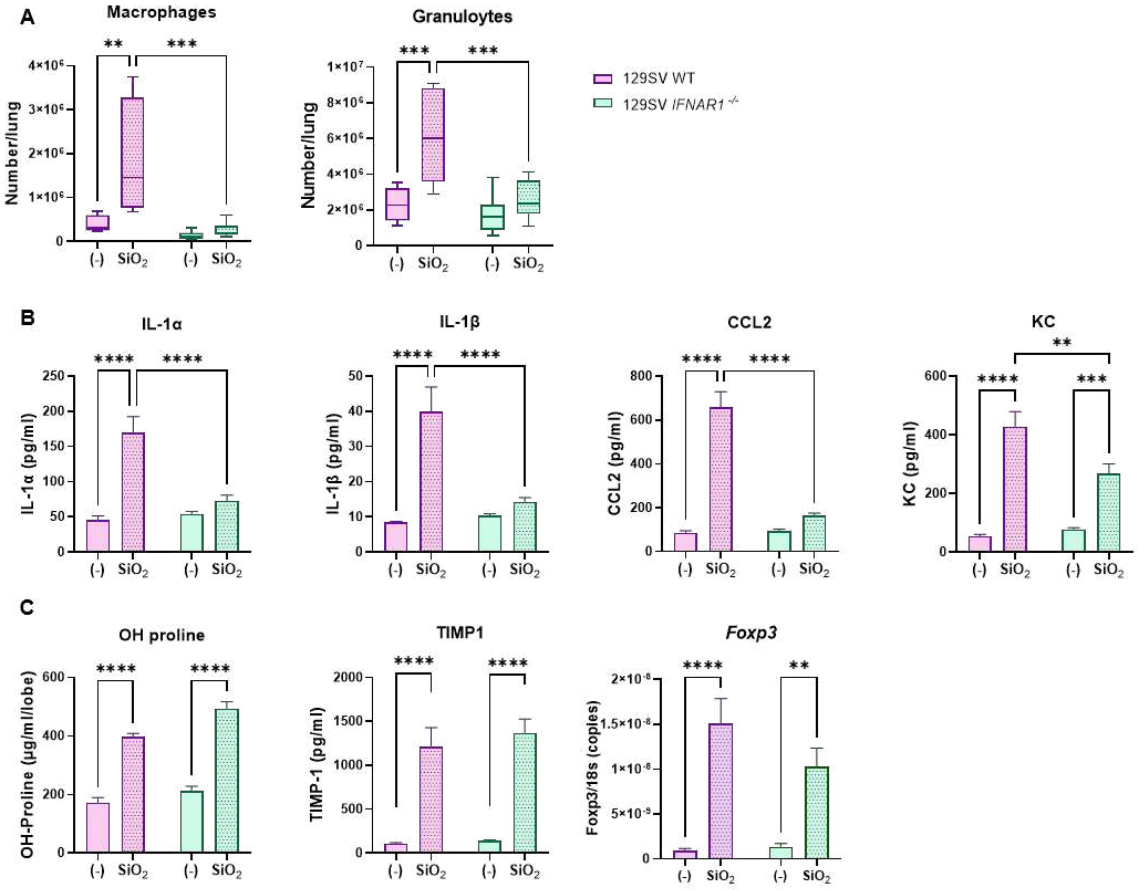



**Figure 1. IFNAR activation is required for sustained IFN-I responses to silica exposure.** 129SV wild-type (WT) and Ifnar1$^{-/-}$ mice received four oropharyngeal aspirations of respirable crystalline silica ($SiO_2$; 1 mg/dose) or saline vehicle (−) over a 6-month period. Irf7 **(A)**, Ifih1 **(B)**, and Oasl2 **(C)** mRNA expression was quantified in lung homogenates at the 6-month endpoint by RT-qPCR. mRNA levels are expressed as copy numbers normalized to 18S rRNA. Data are presented as mean ± s.e.m. (n = 6–12 male mice per group, see table 1). Statistical comparisons were performed using two-way ANOVA with Tukey's post-hoc test. *P < 0.05, **P < 0.01, ***P < 0.001.




511

512 **Figure 2. IFN-I signaling is required for sustained silica-induced pulmonary inflammation without**
513 **promoting fibrosis development.** 129SV wild-type (WT) and *Ifnar1*$^{-/-}$ mice received four oropharyngeal
514 aspirations of crystalline silica ($SiO_2$; 1 mg/dose) or saline vehicle (−) over a 6-month period. **(A)** Myeloid cell
515 recruitment was assessed by flow cytometry, quantifying recruited macrophages
516 ($CD45^+Ly6G^+Ly6C^+F4/80^+CD11c^-CD64^-$) and granulocytes ($CD45^+Ly6G^+Ly6C^+$) in lungs. Data are presented as
517 mean ± s.e.m. (n = 4–10 mice per group, see *table 2*). **(B)** Concentrations of pro-inflammatory cytokines and
518 chemokines (IL-1α, IL-1β, CCL2, and KC/CXCL1) were measured in BALF at the 6-month endpoint. **(C)** Fibrotic
519 markers were evaluated by quantification of hydroxyproline (OH-proline) content in lung tissue, TIMP1 levels in
520 BALF, and *Foxp3* mRNA expression in lung homogenates by RT-qPCR. mRNA levels are expressed as copy
521 numbers normalized to *18S* rRNA. Data are presented as mean ± s.e.m. (n = 6–12 male mice per group, see *table*
522 *1*). Statistical comparisons were performed using two-way ANOVA with Tukey's post-hoc test. *P < 0.05, **P <
523 0.01, ***P < 0.001.

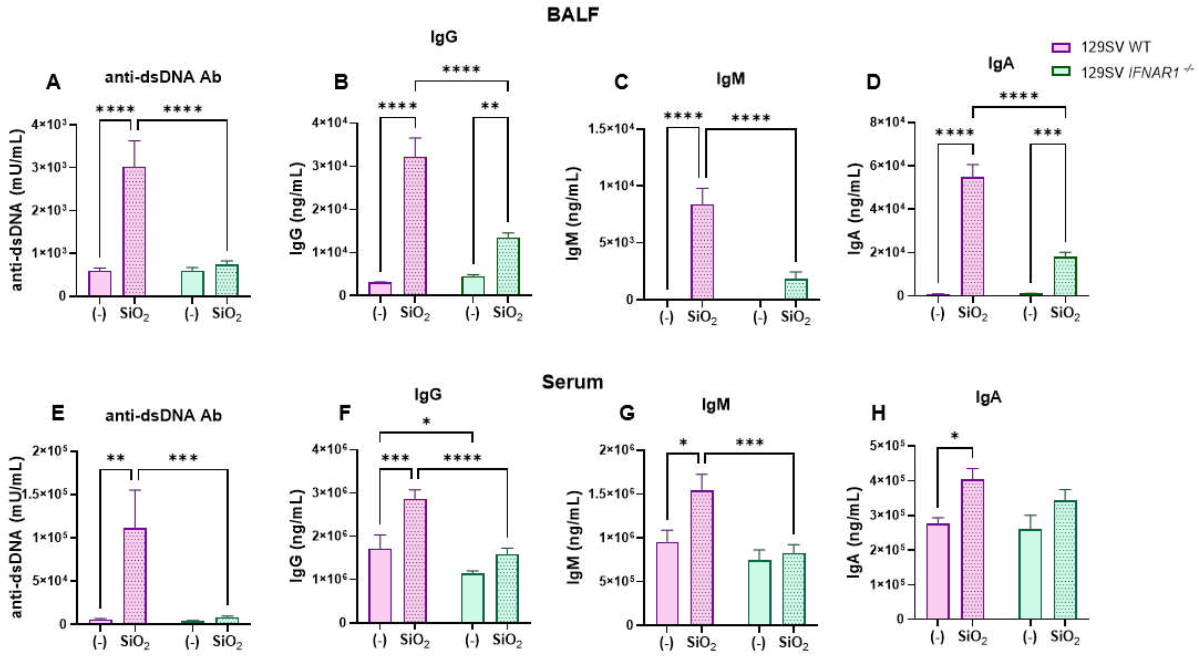



**Figure 3. IFN-I signaling drives silica-induced humoral dysregulation and (auto) antibody production.**

129SV wild-type (WT) and *Ifnar1*$^{-/-}$ mice received four oropharyngeal aspirations of crystalline silica ($SiO_2$; 1 mg/dose) or saline vehicle (−) over a 6-month period. Lung concentrations of anti-dsDNA IgG **(A)**, total IgG **(B)**, IgM **(C)**, and IgA **(D)** were quantified at the 6-month endpoint following BALF collection. Serum concentrations of anti-dsDNA IgG **(E)**, total IgG **(F)**, IgM **(G)**, and IgA **(H)** were quantified at the 6-month endpoint following blood collection. Data are presented as mean ± s.e.m. (n = 6–12 male mice per group, see *table 1*). Statistical comparisons were performed using two-way ANOVA with Tukey's post-hoc test. *P < 0.05, **P < 0.01, ***P < 0.001.

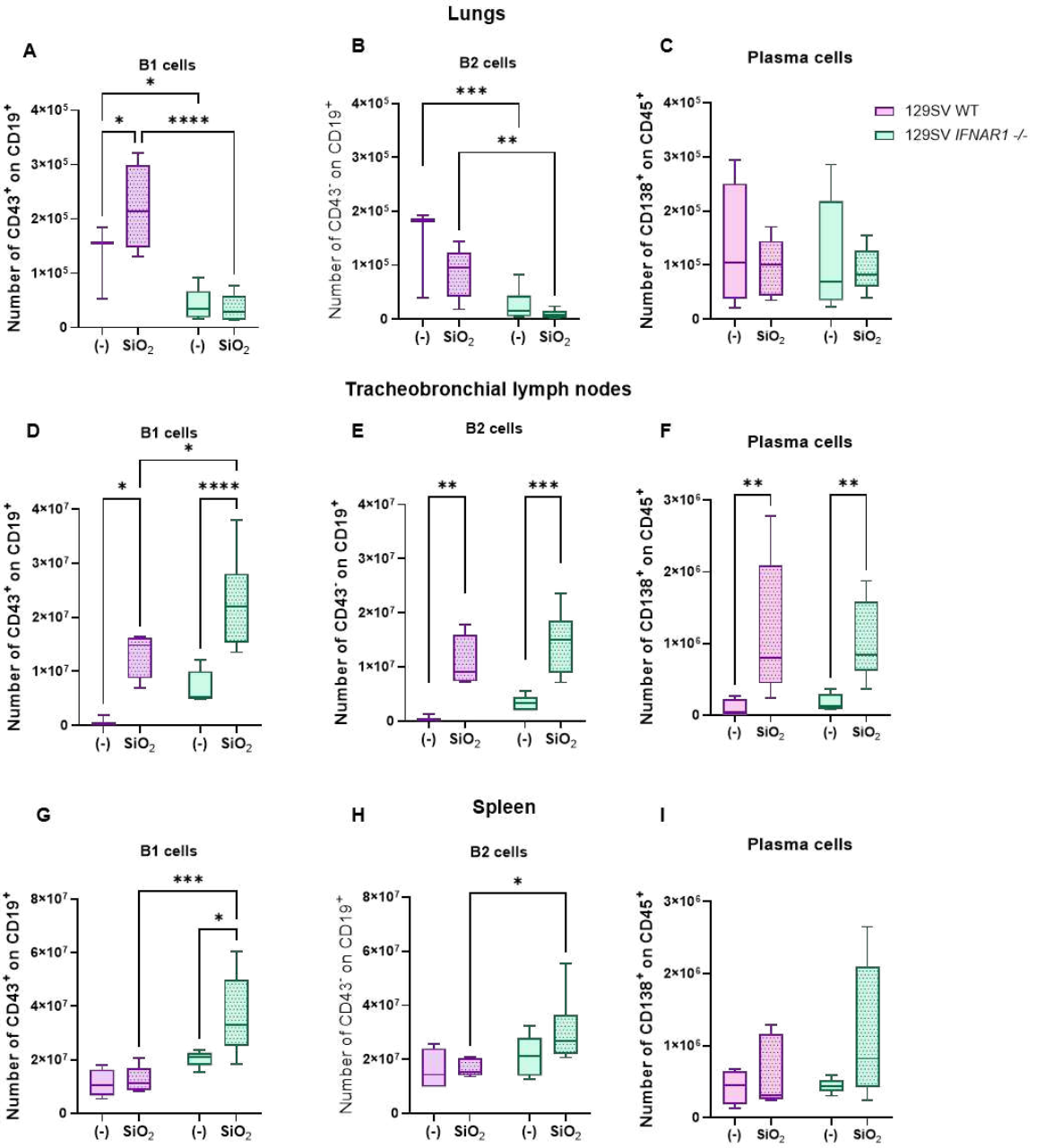



**Figure 4. Silica-induced IFN-I signaling promotes B1 cell subpopulation recruitment to the lungs.**

129SV wild-type (WT) and *Ifnar1*$^{-/-}$ mice received four oropharyngeal aspirations of crystalline silica ($SiO_2$; 1 mg/dose) or saline vehicle (−) over a 6-month period. Single-cell suspensions were prepared from the lungs **(A-C)**, tracheobronchial lymph nodes (TLNs) **(D-F)**, and spleen **(G-I)** of a dedicated male FACS cohort (n = 25). Total B cells were identified as $CD45^+CD19^+CD4^-CD8^-$. B cell subsets were discriminated based on CD43 expression: B1 cells ($CD43^+$), and B2 cells ($CD43^-$). Plasma cells were defined as $CD19^{low/-}$ $CD4^-CD8^-CD138^+$. Data are presented as mean ± s.e.m. (n = 4–10 male mice per group, see *table 2*). Statistical comparisons were performed using two-way ANOVA with Tukey's post-hoc test. *P < 0.05, **P < 0.01, ***P < 0.001.

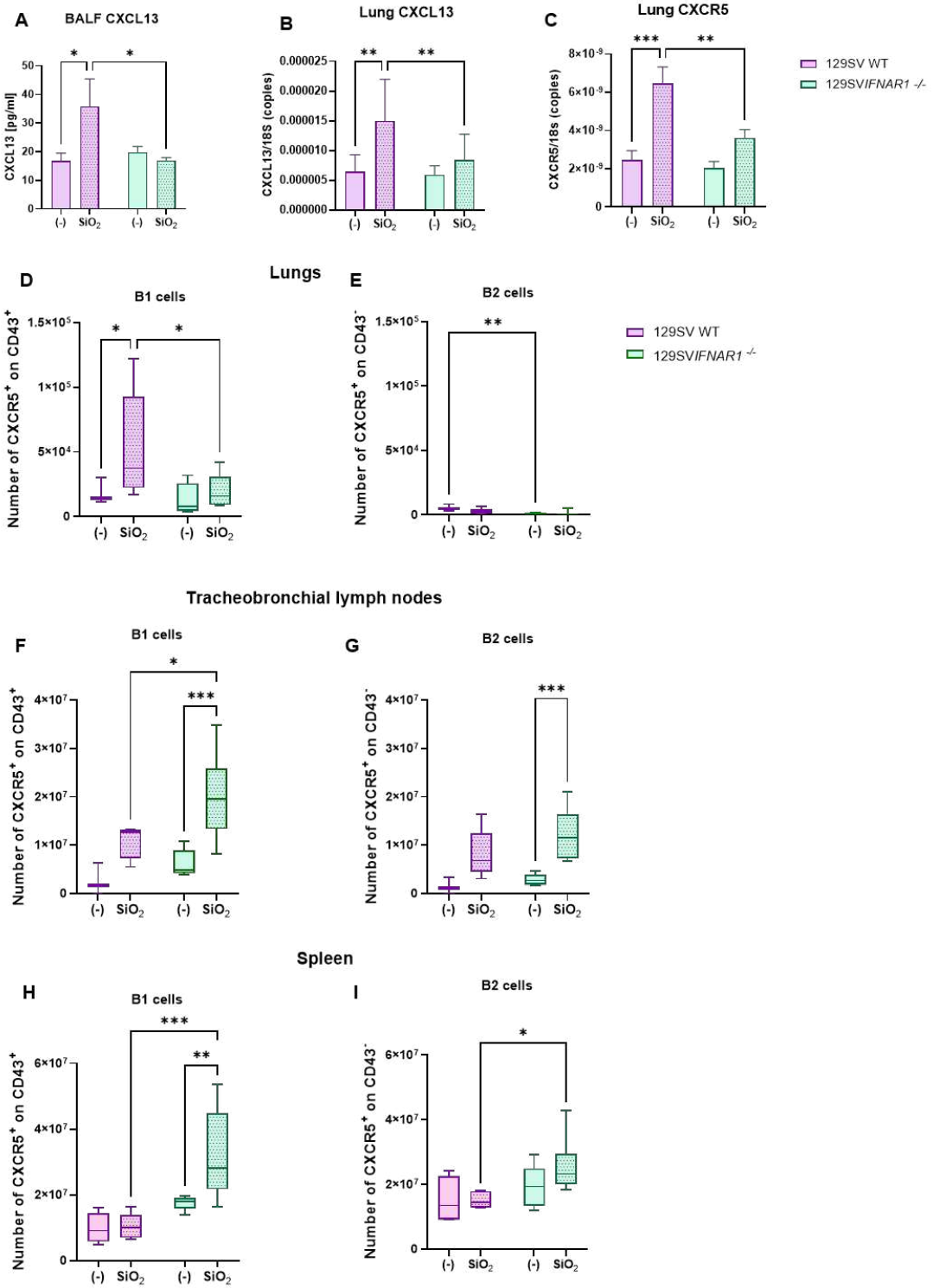
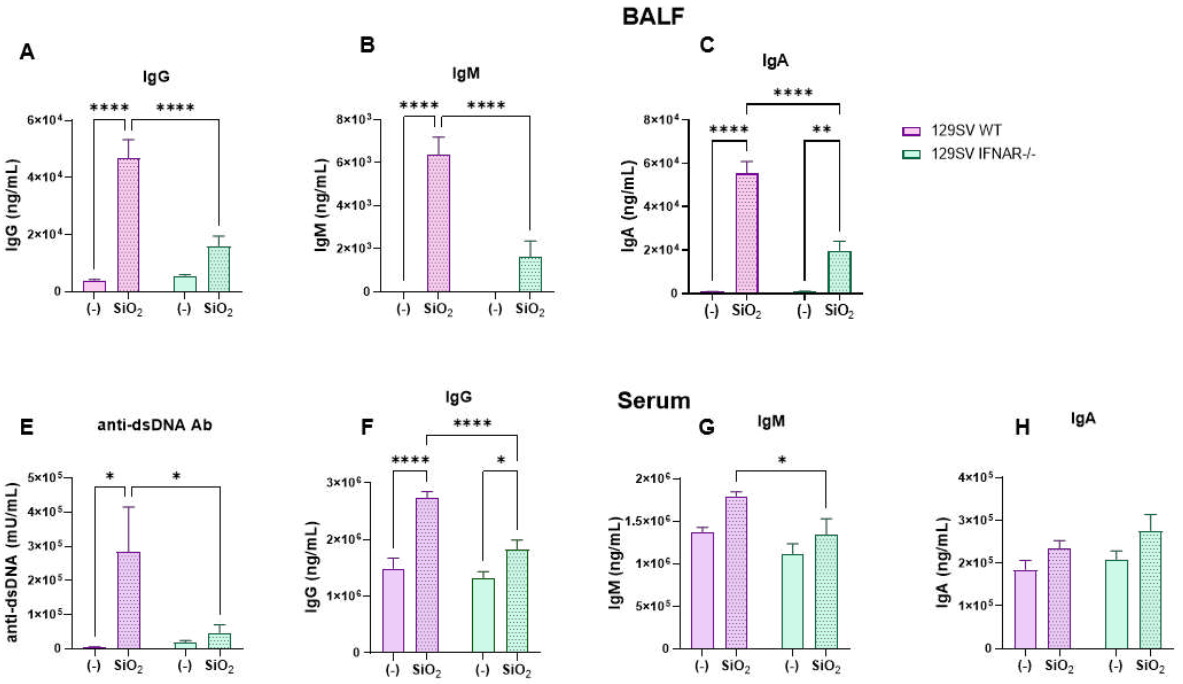



**Figure 5. IFN-I signaling drives the CXCL13/CXCR5 axis and shapes B cell subset distribution in silica-induced pulmonary inflammation.**

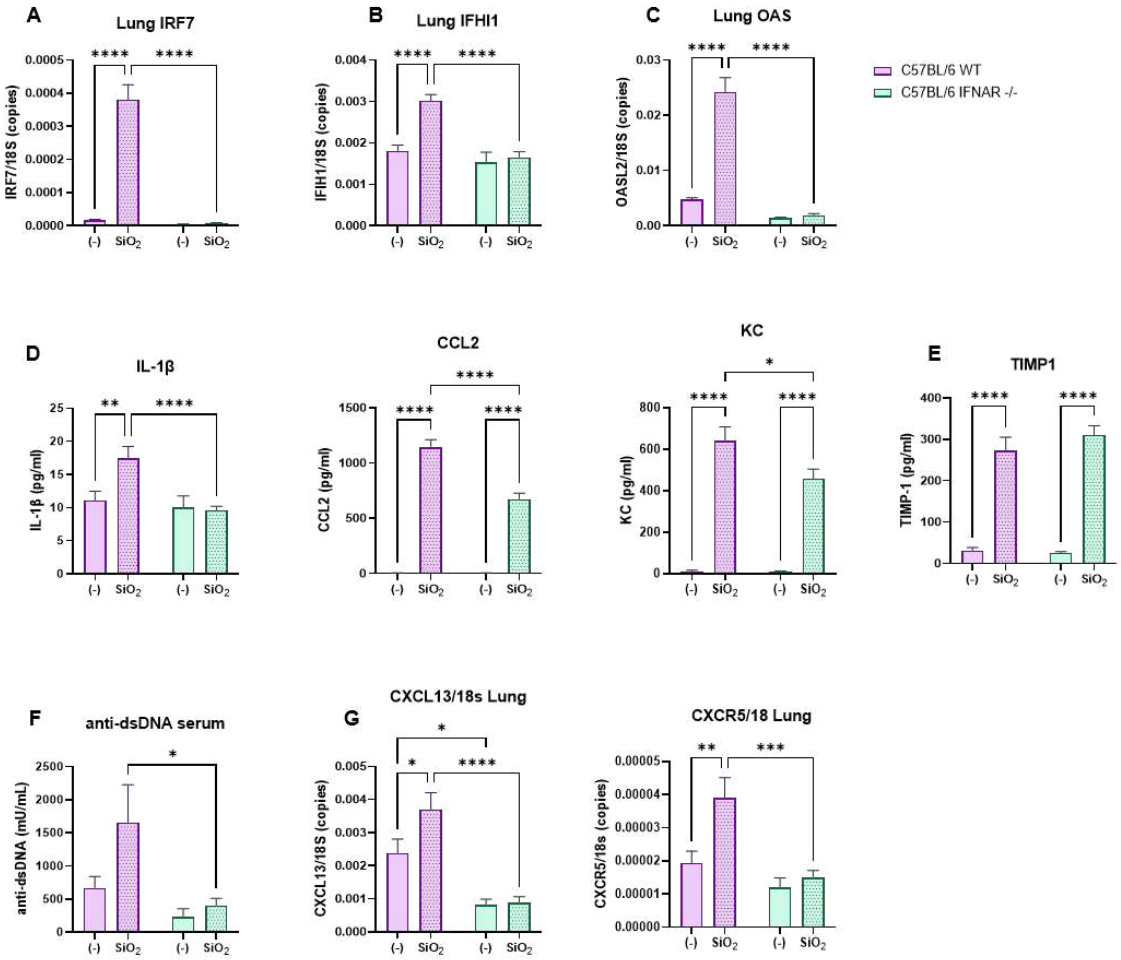
129SV wild-type (WT) and *Ifnar1*$^{-/-}$ mice received four oropharyngeal aspirations of crystalline silica ($SiO_2$; 1 mg/dose) or saline vehicle (−) over a 6-month period. The IFN-I dependency of the CXCL13/CXCR5 axis was assessed at the 6-month endpoint. CXCL13 protein levels were measured in bronchoalveolar lavage fluid (BALF)

**(A)**, and *Cxcl13* **(B)** and *Cxcr5* **(C)** mRNA expressions were quantified in lung homogenates by RT-qPCR. mRNA levels are expressed as copy numbers normalized to *18S* rRNA. Data are presented as mean ± s.e.m. (n = 6–12 mice per group, see *table 1*). **(D-I)** Single-cell suspensions were prepared from the lungs **(D-E)**, tracheobronchial lymph nodes (TLNs) **(F-G)**, and spleen **(H-I)** of a dedicated male flow cytometry cohort (n = 25). Total B cells were identified as $CD45^{+}CD19^{+}$ $CD4^{-}CD8^{-}$. B cell subsets were discriminated based on CD43: B1 cells ($CD43^{+}$), and B2 cells ($CD43^{-}$). CXCR5 was quantified within each B cell subset. Data are presented as mean ± s.e.m. (n = 4–10 male mice per group, see *table 2*). Statistical comparisons were performed using two-way ANOVA with Tukey's post-hoc test. *P < 0.05, **P < 0.01, ***P < 0.001.




**Supplementary Figure 1. Long-term silica instillation promotes IFN-I–dependent humoral dysregulation in female mice.**

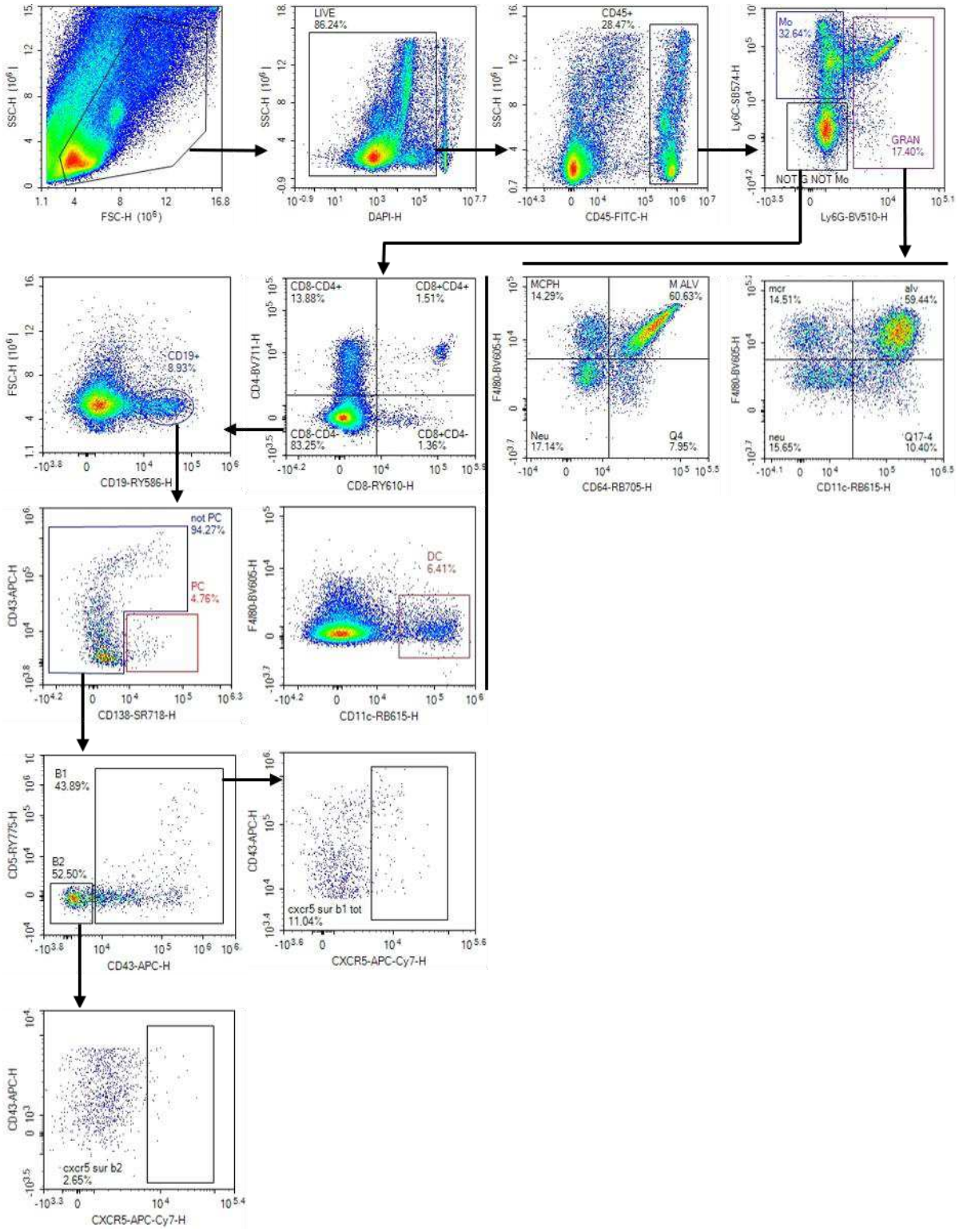
129 SV female wild-type (WT) and *Ifnar1*$^{-/-}$ mice received four oropharyngeal aspirations of crystalline silica ($SiO_2$; 1 mg/dose) or saline vehicle (−) over a 6-month period. Serum concentrations of anti-dsDNA IgG **(A)**, total IgG **(B)**, IgM **(C)**, and IgA **(D)** were quantified at the 6-month endpoint following blood collection. Data are presented as mean ± s.e.m. (n = 6–12 female mice per group, see *table 1*). Statistical comparisons were performed using two-way ANOVA with Tukey's post-hoc test. *P < 0.05, **P < 0.01, ***P < 0.001.




564

565 **Supplementary Figure 2. IFN-I signaling drives the CXCL13/CXCR5 axis and shapes B cell subset**
566 **distribution in silica-induced pulmonary inflammation in C57BL/6 mice.**

567 C57BL/6 wild-type (WT) and *Ifnar*$^{-/-}$ mice received four oropharyngeal aspirations of respirable crystalline silica
568 ($SiO_2$; 1 mg/dose) or saline vehicle (−) over a 6-month period. *Irf7* **(A)**, *Ifih1* **(B)**, and *Oasl2* **(C)** mRNA expression
569 was quantified in lung homogenates at the 6-month endpoint by RT-qPCR. mRNA levels are expressed as copy
570 numbers normalized to *18S* rRNA. Data are presented as mean ± s.e.m. (n = 6–8 male mice per group). **(D)**
571 Concentrations of pro-inflammatory cytokines and chemokines (IL-1β, CCL2, and KC/CXCL1) were measured
572 in BALF at the 6-month endpoint. **(E)** Fibrotic markers were evaluated by quantification of hydroxyproline (OH-
573 proline) content in lung tissue, TIMP1 levels in BALF. **(F)** Serum concentrations of anti-dsDNA IgG was
574 quantified at the 6-month endpoint following blood collection. **(G)** *Cxcl13* and *Cxcr5* mRNA expressions were
575 quantified in lung homogenates by RT-qPCR. mRNA levels are expressed as copy numbers normalized to *18S*
576 rRNA. Data are presented as mean ± s.e.m. (n = 6–8 male mice per group). Statistical comparisons were performed
577 using two-way ANOVA with Tukey's post-hoc test. *P < 0.05, **P < 0.01, ***P < 0.001.




**Supplementary Figure 3. Gating strategy.** A systematic gating hierarchy was applied across all organs. Briefly, total leukocytes were identified by FSC-A/SSC-A, followed by doublet exclusion (FSC-H vs. FSC-A) and dead cell exclusion ($DAPI^-$). Live total leukocytes were identified as $CD45^+$. Within $CD45^+$ population, Granulocytes and Monocytes were discriminated using Ly6G and Ly6C. Inside granulocytes gate, macrophages and neutrophiles were defined by F4/80, CD64 and CD11c. From double negative L6G/Ly6C population, T cells were identified as

584 $CD4^+/CD8^+$, while Dendritic cells were gated as $CD11c^+$. Following these exclusions, B lymphocytes were
585 identified as $CD19^+$, and remaining plasma cells (PC) were excluded with CD138 due to their dim expression in
586 CD19 ($CD19^{low/-}$ $CD4^-CD8^-$ $CD138^+$). B cell compartments were discriminated based on CD43 expression, B-1
587 cells ($CD43^+$), and B-2 cells ($CD43^-$). The frequency of CXCR5 was quantified within each specific B cell subset.
588